Technical Review

No. 4 · 1987

Windows to FFT Analysis (Part II)
Acoustic Calibrator for Intensity Measurement Systems

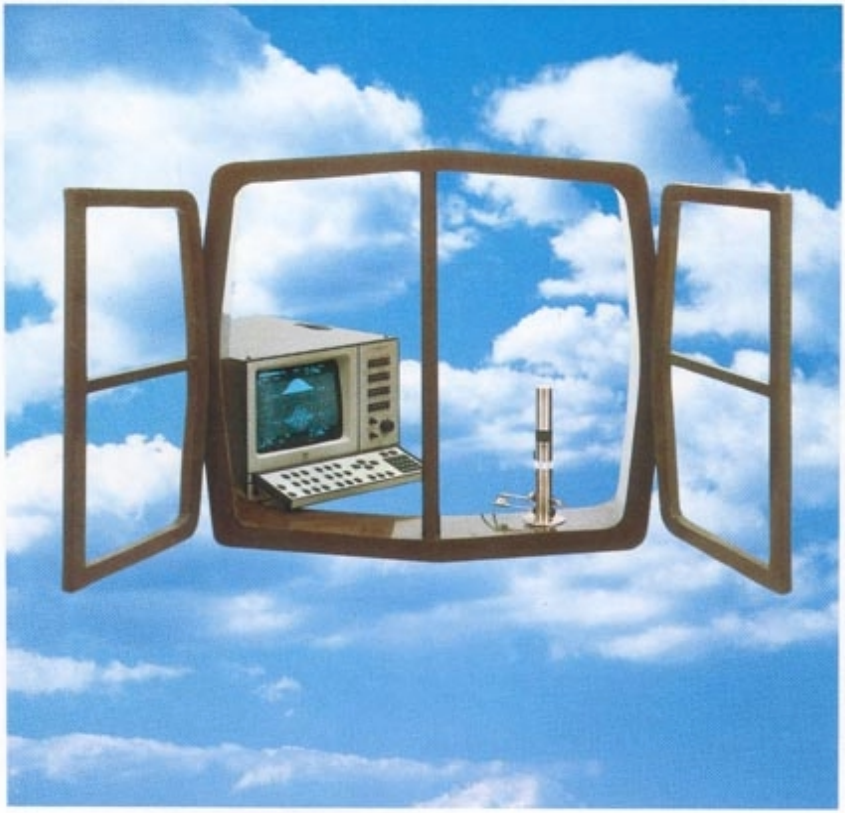

Brüel & Kjær

Previously issued numbers of Brüel & Kjær Technical Review

(Continued on cover page 3)

Technical Review

No. 4 · 1987

Contents

Use of Weighting Functions in DFT/FFT Analysis (Part II)

by Svend Gade and
Henrik Herlufsen

Abstract

Part II of the article "Use of Weighting Functions in DFT/FFT analysis" contains the following Appendices referred to in Part I of the article

A: Analogy between filter analysis and DFT/FFT analysis,
B: Windows and figures of merit,
C: Effective Weighting of overlapped spectral averaging
D: Experimental Determination of the BT product for FFT-analysis using different weighting functions and overlap,
E: Examples of User Defined Windows,
F: Picket Fence Effect

Sommaire

La deuxième partie de cet article, "Application des fonctions de pondération en analyse DFT/FFT", contient les appendices auxquels fait référence la première partie.

A: Analogie entre l'analyse par filtres et l'analyse DFT/FFT.
B: Caractéristiques des fenêtres.
C: Pondération effective des moyennes de spectres avec recouvrement.
D: Determination expérimentale du produit BT en analyse FFT, avec différentes fonctions de pondération et recouvrements.
E: Exemples de fenêtres définies par l'utilisateur.
F: Effet de barrière.

Zusammenfassung

Der zweite Teil des Artikels „Anwendung von Bewertungsfunktionen in der DFT/FFT-Analyse" enthält folgende Anhänge, auf die im ersten Teil Bezug genommen wird:

A: Analogie zwischen Filter-Analyse und DFT/FFT-Analyse

B: Fenster und mathematische Beschreibung
C: Effektive Bewertung bei spekraler Mittelung mit Überlappen
D: Experimentelle Bestimmung des BT-Produkts bei der FFT-Analyse mit verschiedenen Bewertungsfunktionen und Überlappungen
E: Beispiele für anwenderdefinierte Fenster
F: Lattenzauneffekt

Appendix A

Analogy between filter analysis and FFT/DFT analysis

In the time domain a linear filter is described by its impulse response function *h(t)*, which is the response due to an infinitely short and infinitely high unit impulse (so-called Dirac Delta function $\delta(t)$, see Ref. [1]).

By considering any input signal $x(t)$ to the filter as a sum of weighted and time shifted delta functions i.e.

$$x(t) = \int_{-\infty}^{\infty} x(\tau)\,\delta(t-\tau)\,d\tau \tag{A.1}$$

we find, under assumptions of linearity, that the output of the filter is

$$y(t) = \int_{-\infty}^{\infty} x(\tau)\,h(t-\tau)\,d\tau \tag{A.2}$$

or since $h(t) = 0$ for $t < 0$, that

$$y(t) = \int_{-\infty}^{t} x(\tau)\,h(t-\tau)\,d\tau \tag{A.3}$$

The output of a filter at a given point in time t_o is thus determined by the input time history up to time t_o weighted by the impulse response function inverted with respect to time and shifted to t_o i.e. $h(t_o - t)$. This is illustrated in Fig. A.1 for a simple lowpass filter with an exponential decaying impulse response function. The output at time t_o, $y(t_o)$ is the integral (or the area) of the curve in Fig. A.1 d). Mathematically the calculation in eqn.

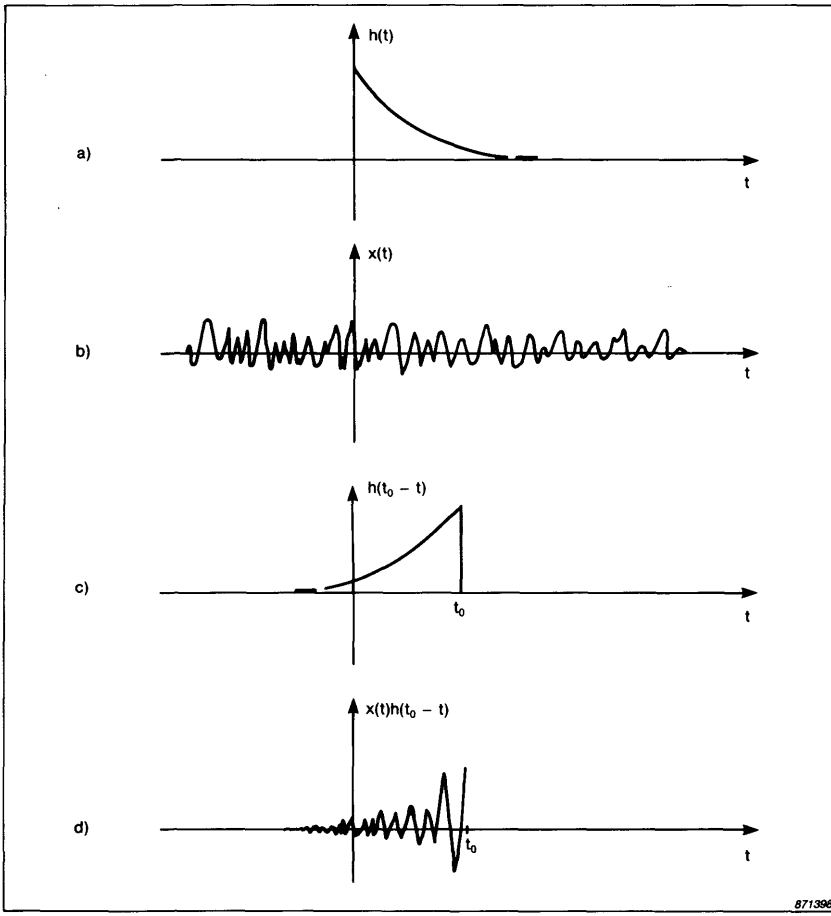

Fig. A.1. a) impulse response of a simple lowpass filter h(t),
b) input signal to be analysed x(t),
c) impulse response inverted and shifted $h(t_o - t)$,
d) weighted input signal to be integrated to give output at time t_o, $y(t_o)$

(A.3) is called convolution of x (t) with h (t) (denoted by x (t) * h(t)). Let us now have a look at the FFT/DFT calculation. To simplify the notation the integral formulation will be used instead of the discrete. The consequence of the discrete form and finite calculation time will be discussed later. Each Fourier spectrum is a transform of the input signal x (t)

applied with a proper weighting function $w(t)$. The transform is based on a time record of length T.

$$Y(f) = \int_{-\infty}^{\infty} x(\tau)\, w(\tau)\, e^{-j2\pi f\tau}\, d\tau = \int_{0}^{T} x(\tau)\, w(\tau)\, e^{-j2\pi f\tau}\, d\tau \qquad \text{(A.4)}$$

$Y(f)$ is the output of the transform at frequency f and at time T (neglecting for the time being the delay due to the calculation time T_{cal}). Considering this output at a certain frequency f_0 as a function of time $Y(f_0,t)$ or just $Y(t)$, we have

$$Y(t) = \int_{t-T}^{t} x(\tau)\, w(\tau-(t-T))\, e^{-j2\pi f_o\left(\tau-(t-T)\right)}\, d\tau \qquad \text{(A.5)}$$

Rewriting this using

$$W_h(t) = w(-t+T) \qquad \text{(A.6)}$$

we get

$$Y(t) = \int_{t-T}^{t} x(\tau)\, w_h\left(-\tau+(t-T)+T\right) e^{j2\pi f_o\left(-\tau+(t-T)\right)}\, d\tau$$

or

$$Y(t) = \int_{t-T}^{t} x(\tau)\, w_h(t-\tau)\, e^{j2\pi f_o(t-\tau-T)}\, d\tau \qquad \text{(A.7)}$$

This is exactly the same equation as for a filter (eqn. A.3) and we can define an equivalent (complex) impulse response function $h_{FT}(t)$ for the Fourier Transform (FT) at frequency f_0 by

$$h_{FT}(t) = w_h(t)\, e^{j2\pi fo(t-T)} \qquad \text{for} \qquad 0 \le t < T \qquad \text{(A.8)}$$

$$h_{FT}(t) = 0 \qquad \text{elsewhere}$$

and (A.7) becomes

$$Y(t) = \int_{t-T}^{t} x(\tau)\, h_{FT}(t-\tau)\, d\tau \qquad \text{(A.9)}$$

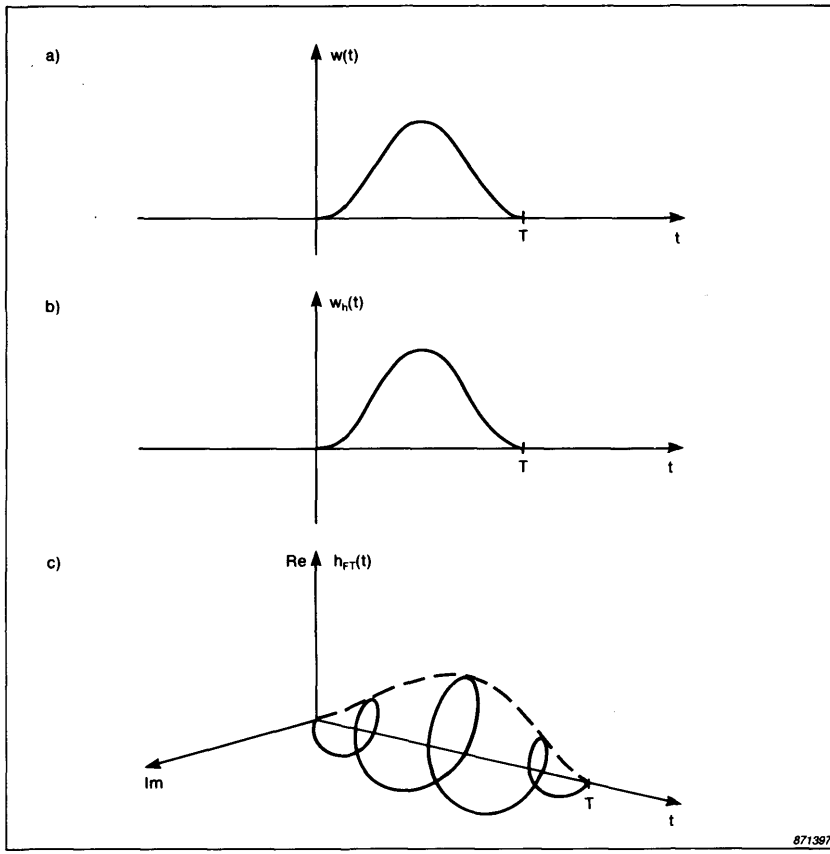

Fig. A.2. a) Hanning Weighting function w(t),
b) $w_h(t) = w(-t + T)$ for the Hanning Weighting,
c) complex impulse response function for filter/line at $f_0 = 4\ \Delta f$ with Hanning Weighting

This proves the analogy between the Finite Fourier Transform eqn. (A.9) and the filtering analysis eqn. (A.3). The impulse response h_{FT} (0 is complex and of finite length T and is determined by the weighting function $w(t)$ (equations (A.8) and (A.6)). Fig. A.2 shows an example of a weighting function and one of the corresponding complex impulse response functions.

Notice that for the commonly used weighting functions like Hanning, Rectangular, Kaiser-Bessel and Flat Top, $w\ (t) = w_h\ (t)$ since they are

symmetrical around $t = {}^{T}/2$ (see also Appendix B eqn. (B.1) and table B.1).

So far we have used an integral formulation of the Fourier Transform. In practical calculations we will of course work with

a) sampled versions of the time signals and their spectra
b) finite calculation time T_{cal} of the transform

The transform which is discrete in both time and frequency domain is called the Discrete Fourier Transform (DFT). The Fast Fourier Transform (FFT) is a fast calculation of the DFT based on a certain algorithm.

re a): The time signals are sampled at time intervals $\Delta t = 1/f_s$, where f_s is the sampling frequency, and the transform will be of N samples which means that $T = N \cdot \Delta t$. The spectrum is computed at discrete frequencies $f_0 = k\ \Delta f = k\ {}^{1}/T$, where k is an integer and $0 \le k < {}^{N}/2$. The transform is thus in its proper form written as:

$$Y(k) = {}^{1}/N \sum_{n=0}^{N-1} x(n)\, w(n)\, e^{-j2\pi kn/N} \qquad \text{(A.10)}$$

x (n) is the n'th time sample in the record, w (n) is the n'th time sample of the weighting function and $Y(k)$ is the spectral value at frequency $k\ \Delta\ f$. The factor ${}^{1}/N$ is just a scaling factor irrelevant for the discussion here.

re b): Since we have a finite calculation time T_{cal} which in most situations is much larger than the sample interval $\Delta\ t$ we will not get a continuous output as with an analog filter or a sample per sample output every $\Delta\ t$ as with a real time digital filter.

Every FFT represents a sample of the Fourier Transform filters (eqn. (A.8) and (A.9)), but the relatively long T_{cal} makes the analysis appear blockwise rather than continuous. In many applications, analysis of transients for instance, it is preferable to look at it as a transform of a data block with various trigger possibilities. This approach will be dealt with later.

In a situation where $T_{cal} \le \Delta t$ (analysis of very low frequencies or analysis with very high zoom factors or much faster calculations than available today) the FFT will be indistinguishable from a bank of real-time digital FIR (finite impulse response) filters with (complex) impulse response functions as given in eqn. (A.8). The FFT is here assumed to work continuously i.e. with free run triggering, as a digital filter.

Since the filtering or FFT is only part of the analysis we will now look at the detector/averager.

The purpose of the detector in a filter analyzer is to measure the power (mean square) of the output signal of the filter $y(t)$, by time averaging of the squared signal $y^2(t)$. The averaging can be linear

$$\overline{y^2} = \frac{1}{T_a} \int_{T_a} y^2(\tau)\, d\tau \tag{A.11}$$

or exponential

$$\overline{y^2}(t) = \frac{1}{\tau_o} \int_{-\infty}^{t} y^2(\tau)\, e^{(\tau - t)/\tau_o}\, d\tau \tag{A.12}$$

which is a continuous running average. The bar indicates average values. For a complete discussion of this subject see Ref. [1].

The averaging in the FFT analyzer is the corresponding summation of the squared amplitudes $|\, Y(i)\,|^2$ of the output samples $Y(i)$, where i is the time or number index. Assuming a transform every T_{cal} we will have the i'th sample at time $t = t_i = i\, T_{cal}$.

This gives for linear averaging

$$\left|\overline{Y}\right|^2 = \frac{1}{N} \sum_{i=1}^{N} \left| Y(i) \right|^2 \tag{A. 13}$$

(see Footnote page 35)

and for exponential averaging

$$\left| Y(i) \right|^2 = 1\, (\left| Y(i) \right|^2 + (^N/2 - 1)\, \left| Y(i-1) \right|^2) \tag{A.14}$$

which is a discrete and recursive form of the analog version eqn. (A.12).

Notice that T_{cal} thus includes calculation of FFT as well as the averaging.

It could now be argued that in order to get a real-time analysis in the sense that all input time samples are equally weighted in the averaging process we need to fulfil the requirement.

$$T_{cal} \leqq \Delta t \tag{A.15}$$

as for real-time recursive digital filtering.

The weighting of the input samples in each power (mean square) calculation $|\, Y(i)\,|^2$ is given by $\left| h_{FT}(t) \right|^2 = w^2_h\, (t)$, and $w_h(t) = w\, (t)$ for the weighting functions considered here as mentioned earlier.

In linear averaging this will result in an effective weighting function $w_{\text{eff}}(t)$ on the time data given by

$$w^2_{\text{eff}}(t) = \frac{1}{N}\sum_{i=1}^{N} w^2\left(t - i\,T_{\text{cal}}\right) \qquad \text{(A.16)}$$

It turns out that if Hanning Weighting is used $w^2_{\text{eff}}(t)$ is uniform (flat) if $T_{\text{cal}} = {}^{T}/_{3}$, ${}^{T}/_{4}$, ${}^{T}/_{5}$, ..., i.e. if 66 ${}^{2}/_{3}$ % overlap, 75% overlap, ... can be performed. This is shown and discussed in **Appendix C.** "True" real-time analysis can thus be performed with Hanning Weighting if

$$T_{\text{cal}} \leqq {}^{T}/_{3}, \qquad \text{(A.17)}$$

is fulfilled.

If Rectangular weighting is used no overlap would be required. This is however as discussed in the article, in general a poor choice of weighting function for continuous signals.

As an example, the B & K Analyzer Type 2032 has a $T_{\text{cal}} \approx 50$ ms in single channel mode with Hanning weighting. This gives the possibility of "true" real-time analysis (with either 66 ${}^{2}/_{3}$ % or 75% overlap) with a 3,2 kHz frequency span setting (i.e. $\Delta f = 4$ Hz, $T = 250$ ms).

After having discussed the analogy between filter and FFT analysis in the time domain and its limitations with respect to real-time operation we will now consider the analogy in the frequency domain.

The relation between input and output in the frequency domain for a filter is

$$Y(f) = H(f) \cdot X(f) \qquad \text{(A.18)}$$

where $X(f)$ and $Y(f)$ are the spectra of the input and output signals respectively and $H(f)$ is the frequency response of the filter. This is a consequence of eqn. (A.3) and the convolution theorem for the Fourier Transform (Refs. [1,7,8]). $H(f)$ is the Fourier Transform of $h(t)$

$$H(f) = F\{h(t)\} \qquad \text{(A.19)}$$

and is called the (complex) filter characteristic, containing both amplitude and phase information.

From eqn. (A.8) we thus find that the filter characteristic for the FFT at frequency f_0 is given by

$$H_{FT}(f) = F\{w(t)e^{j2\pi f_o(t-T)}\} \quad \text{(A.20)}$$

since $w_h(t) = w(t)$ for the weighting functions considered here.

Defining

$$F\{w(t)\} = W(f) \quad \text{(A.21)}$$

we have that

$$H_{FT}(f) = F\{w(t)\, e^{j2\pi f_o(t-T)}\} = W(f-f_o) \quad \text{(A.22)}$$

The filter characteristic for the filter/line at frequency f_0 is thus the Fourier Transform of the weighting function shifted to the relevant frequency f_0. The FFT can thus be considered as a bank of parallel, identical constant bandwidth filters with the amplitude characteristic $|W(f - f_0)|$ i.e. $|W(f)|$ I centered at the frequency f_0. This is the basis for the plots of the filter amplitude characteristics for the different weighting functions (Fig. 6, 8, 11 and 15) in Part I of this article.

For analog filters the characteristics are always complex conjugate symmetric about $f = 0$ i.e. $H(-f) = H^*(f)$. This is not true for $W(f - f_0)$, where $f_0 \neq 0$, and the FFT output $Y(i)$, for $f_0 \neq 0$, is in general complex.

The phase characteristic of the FFT filters is given by the phase of $W(f)$, $\angle W(f)$. For the weighting functions considered here which are symmetric about $t = T/2$ the phase is given by the time shift of $T/2$ as

$$\angle W(f) = -2\pi f T/2 = -\pi f T = -\pi f / \Delta f \quad \text{(A.23)}$$

or

$$\angle W(f - f_o) = -\pi (f - f_o) / \Delta f \quad \text{(A.24)}$$

The phase characteristic is linear with a shift of $-\pi$ for every Δf (filter/line spacing) see Fig. A.5 b). (A linear phase characteristic is often a main advantage in application of FIR filters).

As already mentioned another approach for the formulation of the FFT is very often used. This approach is based on the blockwise analysis and that the FFT line spectrum is considered as the Fourier Series of a periodic signal with the data block (record) being one period. The derivation of the FFT from the Integral Fourier Transform is given by the following steps:
a) time sampling, b) time multiplication - frequency convolution, c) frequency sampling. This is dealt with in detail in Refs. [4 and 7].

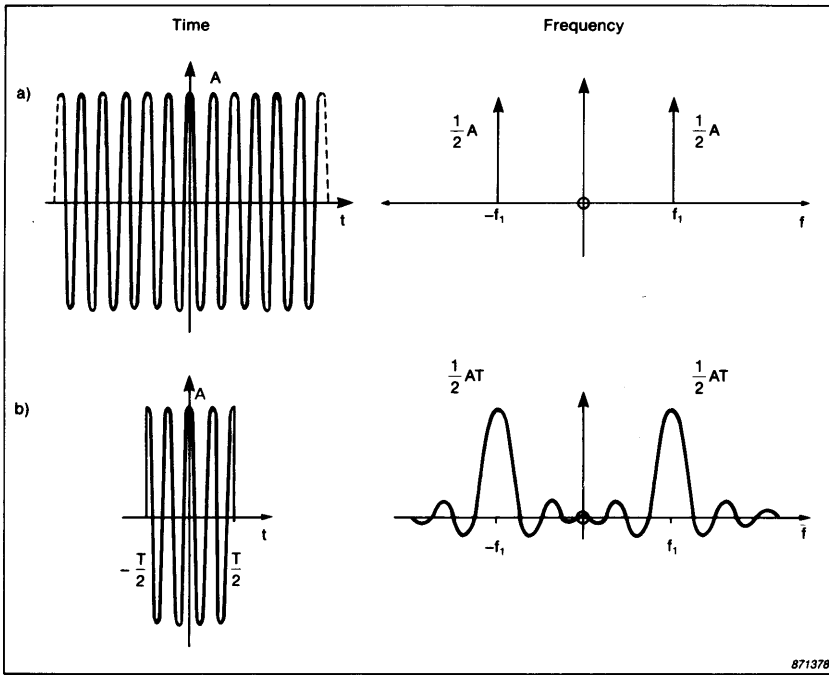

Fig. A.3. Frequency spectrum of a) a sinusoidal time signal and b) the tone burst produced by truncating the time signal in a)

Let us here take an example and see the differences and similarities of the two formulations. The signal to be analyzed is the cosine,
$x(t) = A \cdot \cos(2\pi f_1 t)$ with a Fourier Spectrum as shown in Fig. A.3.a).

Truncation of the signal by multiplication with Rectangular weighting of length T, produces the tone burst shown in Fig. A.3.b). The effect of this multiplication is a convolution in the frequency domain of the spectrum in Fig. A.3.a) with the spectrum of the Rectangular window
$W(f) = T \frac{\sin(\pi f T)}{\pi f T}$ resulting in the spectrum shown in Fig. A.3.b). The convolution is written as

$$X(f) \star W(f) = \int_{-\infty}^{\infty} X(f') \cdot W(f-f')\,df' \qquad \text{(A.25)}$$

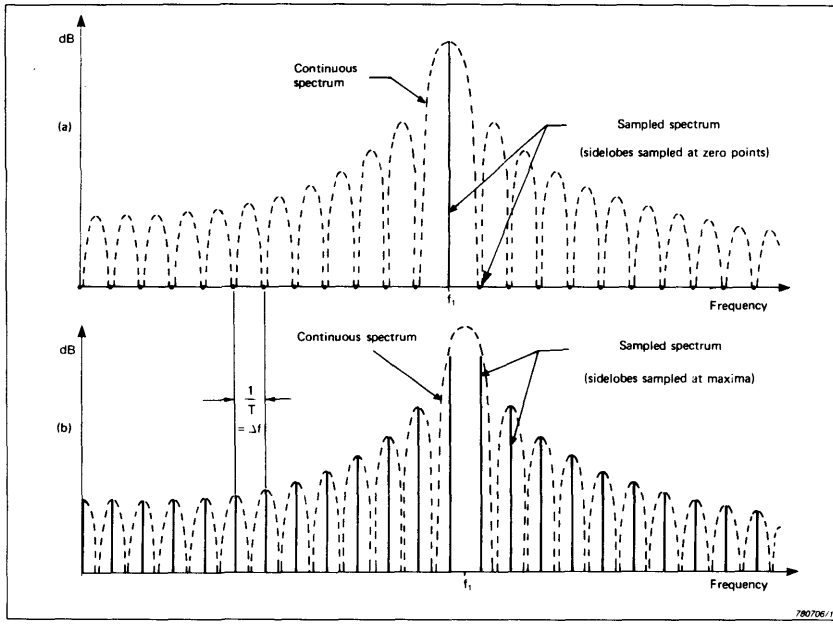

Fig. A.4. Frequency sampling of the continuous spectrum of the time limited sinusoid. Number of periods within the time window (record length) is a) integer (12) b) half-integer (12 $^1/_2$)

which can be interpreted as a swept filter analysis where $W(f_0 - f)$ is the filter characteristic.

The continuous spectrum is calculated i.e. sampled at the discrete frequencies $f = k\,\Delta f = k\,{}^1/_T$. Depending upon the frequency f_1 we will get different results as exemplified in Fig. A.4. In Fig. A.4.a) f_1 coincides with one of the samples, here $f_1 = 12\,\Delta f$ (corresponding to 12 periods in the record length T), and we get only one line with the correct amplitude in the FFT spectrum. In Fig. A.4.b) however f_1 is in between two samples, here $f_1 = 12\ 1/2\,\Delta f$ (corresponding to 12 1/2 periods in the record length T) and all the side lobes will appear in the analysis and the maximum amplitude is too low. This is also referred to as leakage.

Returning to the filter analogy let us consider a bank of filters at $f_0 = k\,\Delta f$ with filter characteristics $W\,(f - f_0)(= W(f_0 - f))$ to give the same results as convolution and sampling. In Fig. A.5 it is shown how the output *Y(i)* is found using the filter model (*i* is the time index as defined

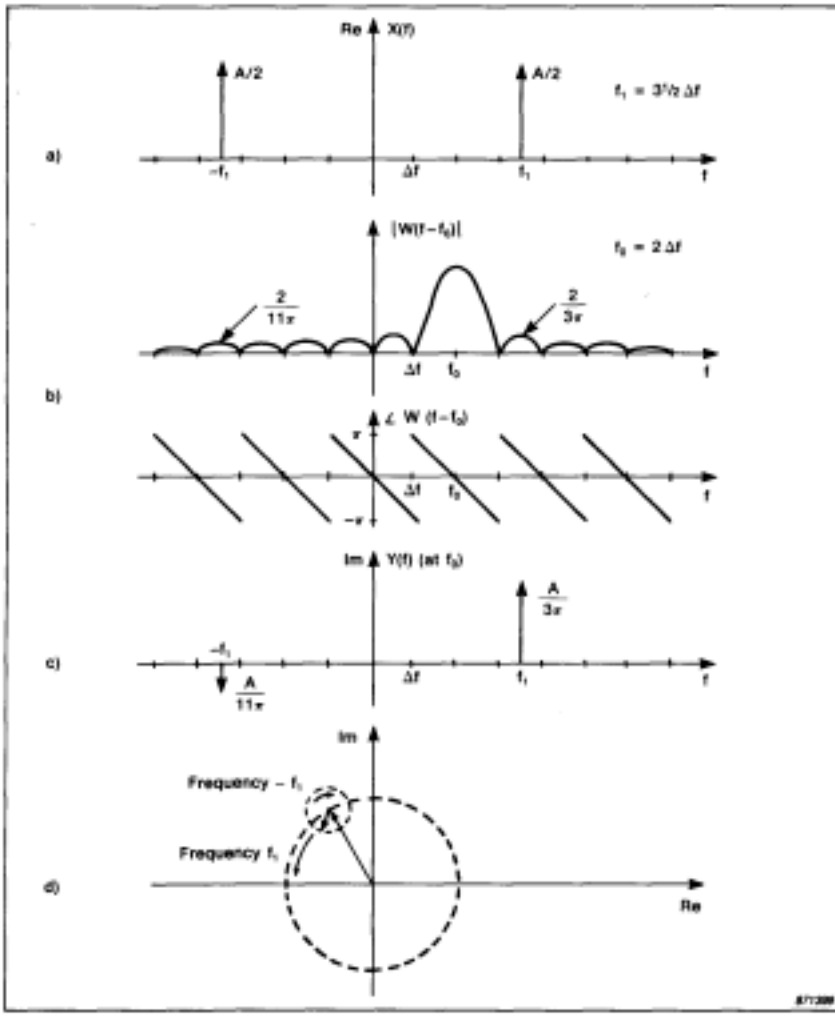

Fig. A.5. a) Spectrum of input time signal x(t) = A cos (2 π f 1t), f_1 = 3 1/2 Δf,

b) amplitude and phase characteristic of filter/line at f_0 = 2 Δf, with rectangular weighting,

c) Spectrum of output signal for filter/line f_0= 2 Δf,

d) complex time output signal for filter/line f_0 = 2 Δf (sum of contra-rotating vectors with frequency of f_1 and -f_1 respectively)

earlier). The input signal is in this example a cosine with frequency f_1 = 3 1/2 Δf and the filter considered is at f_0 = 2 Δf as shown in Fig. A.5 a) and b). The complex filter output at f_0 = *2* Δf in the frequency domain and in the time domain is shown in Fig. A.5 c) and d) respectively. $|Y(i)|$ will vary between

$$|Y(i)|_{max} = \frac{A}{3\pi} + \frac{A}{11\pi} \text{ and } \quad |Y(i)|_{min} = \frac{A}{3\pi} - \frac{A}{11\pi}$$

which means $\frac{|Y(i)|_{max}}{|Y(i)|_{min}}$ = 1,75 (corresponding to 4,9 dB).

The maxima are found when the two contra-rotating vectors point in the same direction and the minima when they point in opposite directions.

This varying amplitude can be seen on the FFT analyzer when analyzing a sinusoid with free run trigger and Rectangular weighting (see Ref. [4] Fig. 8 for inst.).

In the other model this is explained by changing the phase of the input signal relative to the window, i.e truncating at different points in time. Truncating at a zero crossing of the sinusoid instead of at a maximum will give a different tone burst and a corresponding different spectrum than shown in Fig. A.3 b). The sidelobes of the sin *x/x* will add at low frequencies and subtract at high frequencies instead of subtract at low frequencies and add at high frequencies as in Fig. A.3 b). This is discussed in detail in Ref. [4].

Conclusion

The filter analogy of the FFT has been discussed and is a practical tool in many situations to better understand certain phenomena and is used extensively in this article. The limitation in the analogy with respect to real-time considerations has been pointed out as well and should be kept in mind.

The other formulation based on time multiplication - frequency convolution and sampling has proven to be a very convenient and a preferable model in several other applications of FFT.

It should be noted that these models or mathematical formulations are developed for understanding the FFT techniques. They are valid within their limitations and neither one should be considered superior to the other.

Appendix B

Windows and Figures of Merit

The mathematical formulation of the Weighting Functions used in the B & K Analyzers Types 2032 and 2034 is as follows:

$$w(t) = a_0 - a_1 \cdot \cos 2\pi t/T + a_2 \cdot \cos 4\pi t/T - a_3 \cdot \cos 6\pi t/T + a_4 \cdot \cos 8\pi t/T$$

$$= a_0 - \sum_{i=1}^{2} a_{(2i-1)} \cdot \cos 2\pi (2i-1) t/T + \sum_{i=1}^{2} a_{(2i)} \cdot \cos 2\pi (2i) t/T \quad \text{(B.1)}$$

for $0 \leqq t < T$

$w(t) = 0$ elsewhere

except for Transient and Exponential Weighting.

As can be seen the windows consist of a sum of a DC and four harmonic terms. The coefficients of the 4 standard windows implemented in the 2032 and 2034 are given in Table B.I.

	a_0	a_1	a_2	a_3	a_4
Rectangular	1	-	-	-	-
Hanning	1	1	-	-	-
Kaiser-Bessel	1	1,298	0,244	0,003	-
Flat Top	1	1,933	1,286	0,388	0,032

Table B.1. Window coefficients

Maximum Amplitude

The max. amplitude can be calculated from the sum of the window coefficients.

$$\textbf{Max}\ w(t) = \sum_{i=0}^{n} a_i \quad \text{(B.2)}$$

Another relevant quantity for windows, sometimes called the Coherent Gain, is

Coherent Gain = a_0/Max $w(t)$ (B.3)

This quantity indicates the reference amplitude gain of the filter characteristic if the maximum amplitude (Max. $w(t)$) was unity.

In 2032/34 all windows are scaled in such a manner that the "area" under the weighting function is equal to one ($a_0 = 1$). This corresponds to a reference gain of unity which ensures no power spectral bias error for a sinusoid with a frequency coinciding with one of the centre frequencies/ lines of the filters.

Effective Duration

The effective duration of the window is calculated from

$$T_{\text{eff}} = \frac{1}{(\text{Max } w(t))^2} \int_0^T w^2(t)\ dt \qquad \text{(B.4)}$$

By use of (B.2) and Parseval's theorem, for the weighting function considered as a periodic function with period T, the effective duration can be calculated from the square of the window coefficients by

$$T_{\text{eff}} = \frac{a_0^2 + 2\sum_{i=1}^{n} \left(\frac{a_i}{2}\right)^2}{\left(\sum_{i=0}^{n} a_i\right)^2} \cdot T \qquad \text{(B.5)}$$

The effective duration can be interpreted as a measure of the energy (integral of values squared) of the weighting function $w(t)$ normalized with the maximum amplitude Max. $w(t)$.

Effective Noise Bandwidth

The Effective Noise Bandwidth (ENBW) is defined as

$$\text{ENBW} = \frac{\int_{-\infty}^{\infty} |W(f)|^2\ df}{\text{Max } |W(f)|^2} \qquad \text{(B.6)}$$

Using Parseval's theorem we find the definition in the time domain given by

$$\mathrm{ENBW} = \frac{\int_0^T w^2(t)\,dt}{\left(\int_0^T w(t)\,dt\right)^2} \tag{B.7}$$

Again using Parseval's theorem for the weighting function considered as a periodic function with period T as previously we find, since

$$\int_0^T w(t)\ dt = a_0 T \tag{B.8}$$

that

$$\mathrm{ENBW} = \frac{\left(a^2{}_0 + 2\sum_{i=1}^{n}\left(\frac{a_i}{2}\right)^2\right)\ T}{a^2{}_0 T^2} = \frac{a_0^2 + 2\sum_{i=1}^{n}\left(\frac{a_i}{2}\right)^2}{a_0^2} \cdot \Delta f \tag{B.9}$$

The reciprocal of ENBW is sometimes in the literature called the Processing Gain (PG), since an increased noise bandwidth permits additional noise to contribute to a spectral estimate, giving a lower signal to noise ratio, when detecting sinusoidal signals in noise.

Overlap Correlation

If windows are applied to non-overlapping partitions of a time sequence, a significant part of the time signal is ignored due to the fact that most windows exhibit small values near the boundaries. To avoid this loss of data, overlap analysis can be performed.

In 2032/34 standard overlap of 0%, 50%, 75% and maximum can be chosen.

The correlation as a function of fractional overlap, *r* can be calculated using the correlation coefficient.

$$c(r) = \frac{\int_0^T w(t) \cdot w\left(t + (1-r)\,T\right) dt}{\int_0^T w^2(t)\,dt} \tag{B.10}$$

Correlation Coefficient	25% Overlap	50% Overlap	75% Overlap	100% Overlap
Rectangular	0,25	0,5	0,75	1
Harming	0,0075	0,1667	0,6592	1
Kaiser-Bessel	0,0014	0,0735	0,5389	1
Flat Top	0,0005	-0,0153	0,0455	1

Table B.2. Correlation coefficients for 25%, 50%, 75% and 100% overlap for the various window functions

The correlation coefficients for 25%, 50%, 75% and 100% overlap are shown in Table B.2.

For an estimate based on the average of a number *n#d* of statistically independent records (or degrees of freedom) the BT-product (Bandwidth times Averaging Time) per filter is equal to the number of averages independent of the weighting function used

$$BT = n_d \tag{B.11}$$

Thus the relative standard deviation, $\in_r$ for autospectra (RMS) of gaussian random signals is

$$\in_r = \frac{1}{2\sqrt{BT}} = \frac{1}{2\sqrt{n_d}} \tag{B.12}$$

In an analysis with average of n_d records with 50% overlap the BT-product is given by (Refs. [2 and 3])

$$BT_{50\%} = [[1+2c^2(50\%)]/n_d - 2c^2(50\%)/n^2_d]^{-1} \tag{B.13}$$

and for 75% overlap the BT-product is given by (Refs. [2 and 3]).

$$BT_{75\%} = [[1+2c^2(75\%) + 2c^2(50\%) + 2c^2(25\%)\ \}/n_d$$

$$- 2\,[c^2(75\%) + c^2(50\%) + 3c^2(25\%)\ ]/n^2_d]^{-1} \tag{B.14}$$

The negative terms in B.13 and B.14 are edge effects of the average and can be ignored if the number of averages, n_d is larger than ten. Also note

that for most windows the correlation (squared) for 25 % overlap is small compared to 1 and can also be omitted from B.14 without significant error.

The effective BT-product per filter per record BT_{eff}. shown in Table 3 (in Part I of this article) is now calculated from

$$BT_{eff}\,(50\%) = BT_{50\%}/n_d \qquad \text{(B.15)}$$

and

$$BT_{eff}\,(75\%) = BT_{75\%}/n_d \qquad \text{(B.16)}$$

The theoretical values have been verified experimentally (see **Appendix D).**

An example: for a white noise gaussian random signal 123 spectra have been averaged using Hanning Weighting with 75% overlap. What is the difference in dB between the maximum and minimum values in the auto-spectrum estimate?

From Table 3 we have the effective BT-product to be $123 \cdot 0{,}52 = 64$. From (B.12) the relative standard deviation (68% confidence interval) is 1/16 or 0,5 dB. The 99% confidence interval is given by ± three times the standard deviation. Assuming that the maximum and minimum values of the spectral estimate will be the extremes of the 99% confidence interval we will have a difference between the maximum and minimum values of $2 \cdot 3 \cdot \in_r$, i.e. here 3 dB.

Appendix C

Effective Weighting of Overlapped Spectral Averaging

The effective weighting of an overlapped spectral average analysis can be defined as the variation of the spectral level from an impulse versus the impulse's position in time - that is the weight given to the data in the spectral average as a function of time. For example, for 50% overlap, linear averaging and Hanning window a weighting as shown in Fig. C.I is obtained. The Figure of interest here is the ripple on the spectral level, which can be defined as 10 log (Max/Min) - in the above example 3 dB.

The effective weighting is relatively easy to calculate numerically by summing a series of squared weighting functions with the specified overlap (see **Appendix A** eqn. (A.16)). The ripple periodicity must by symmetry be the same as the shift between spectra.

A case of interest is the effective weighting function obtained in overlap analysis with Hanning window applied. The ripple obtained as a function of shift between records is shown in Fig. C.2. As can be seen the ripple falls very rapidly from 3 dB for a shift of 0,5 to zero between shifts of 0,3 and 0,4. Additional zeroes are seen for smaller shifts. These actually lie in the series $^1/_3$, $^1/_4$, $^1/_5$, $^1/_6$ etc., i.e. $^1/_{(\text{integer}>2)}$.

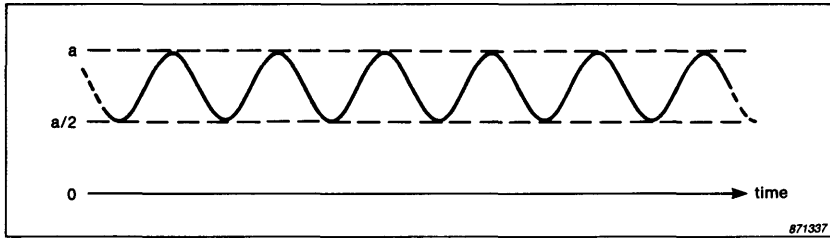

Fig.C.1. Ripple in the effective weighting of the time signal when using Hanning Weighting and 50% overlap

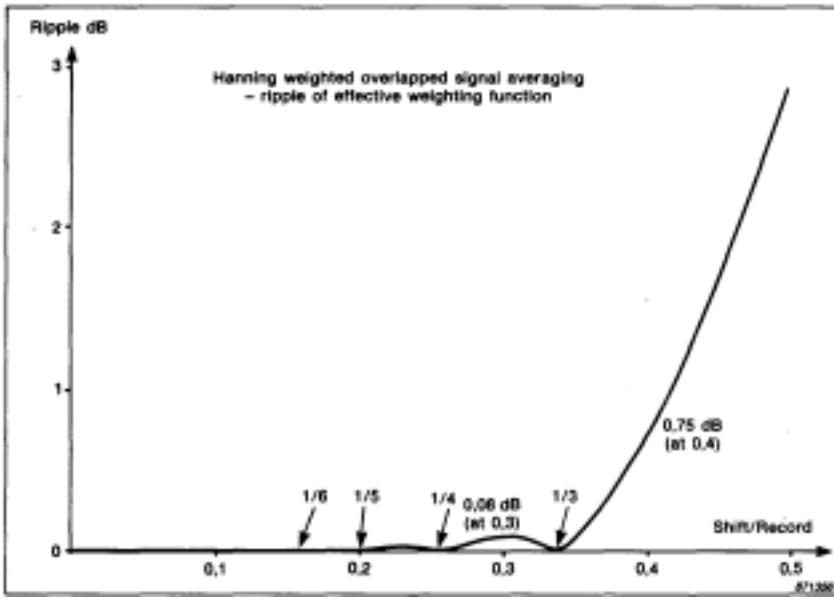

Fig.C.2. Ripple of effective weighting function using Hanning weighted overlapped signal averaging

Among other things this means that the widest analysis bandwidth for overlapped averaging to obtain a uniform weighting is found with an overlap of $^2/_3$. While $^2/3$ is not a practical shift given the normal FFT size the nearest value is quite good enough.

This situation comes about in the following manner. The squared Hanning has a form $[1 - \cos (2 \pi {}^t/_T)]^2$ i.e. contains only a constant and the terms $\cos (2 \pi t/T)$ and $\cos (4 \pi t/T)$, where T is the window length. The shift of the window is equivalent to a phase shift of A for the $\cos (2 \pi t/T)$ term and $2A$ for the $\cos (4 \pi t/T)$ term. Considering the series of windows which affect a given impulse, the ripple is contained in these cos terms and the contribution for each term can be considered as the real part of a complex addition - the example for two windows separated by A is shown in Fig. C.3.a.

It is seen in Fig. C.3.b that when the shift is 0,5 of the window length, i.e. the phase shift $A = \pi$, the sum of only the terms with phase difference A is zero.

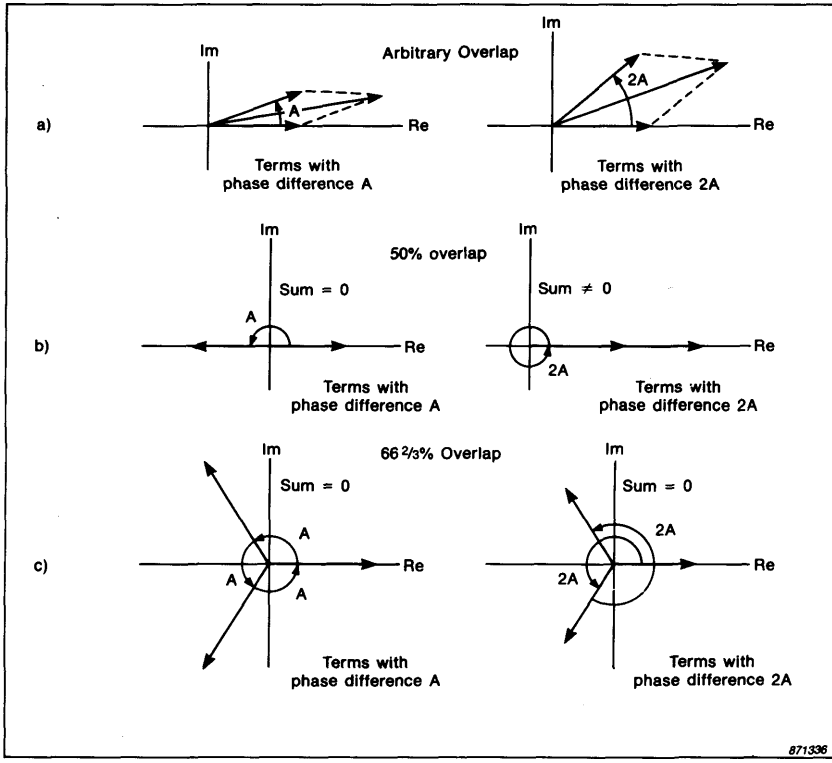

Fig.C.3. Addition (complex) of the terms with phase difference A and 2A in calculation of the ripple of the effective weighting function in situation with overlapping and Hanning

But when a shift of $^1/_3$ is used the sum of both the terms with phase difference *A* and 2 *A* are zero and likewise for any shift of $^1/_{(\text{integer}>2)}$.

Thus the overlap must be $^2/_3$, $^3/_4$, $^4/_5$, $^5/_6$ etc. (see Fig. C.4) to obtain results equivalent to a true real-time analysis with parallel filters (Refs. [1,5 and 6] and **Appendix A**).

75% overlap is the most commonly used overlap, since it is an integer number of samples when the transform size is a power of two.

Using special parameter number 2 in 2032/34 an overlap of 1365 samples corresponding to nearly $^2/_3$ record length can be specified, thus giving a nearly flat weighting in the widest analysis bandwidth possible.

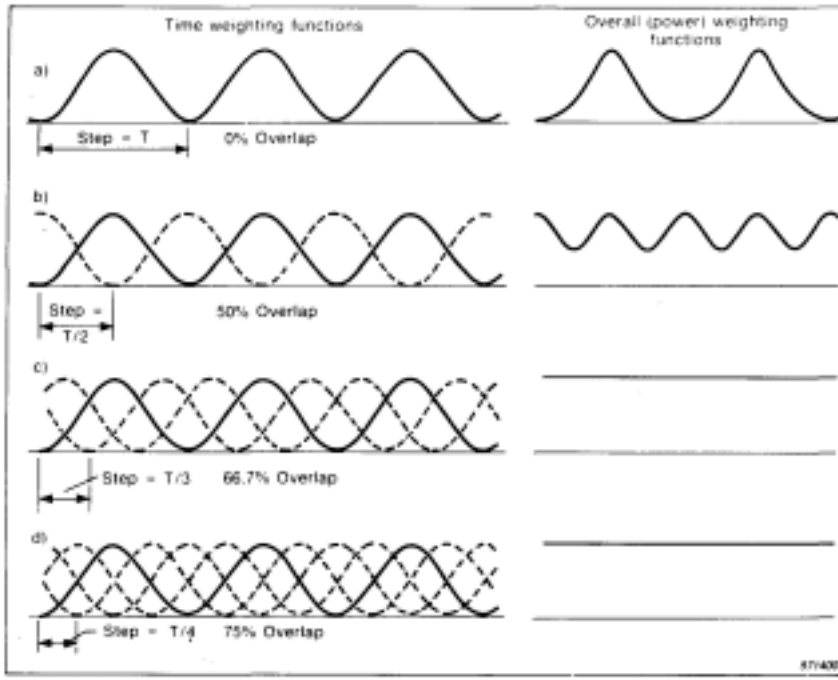

Fig. C.4. Overall weighting functions for overlapping Hanning windows

Appendix D

Experimental Determination of the BT-Product for FFT-Analysis using different weighting functions and overlap

The BT-product is determined from the relative standard deviation, $\in_r$ of the amplitude of auto-spectra estimates when analyzing a gaussian white noise random signal.

For RMS values we have

$$\in_r = \frac{1}{2 \cdot \sqrt{BT}} \Leftrightarrow \; BT = \frac{1}{4 \cdot \in_r^2} \tag{D.1}$$

which means that we can determine the BT-product from experimentally determined standard deviations of autospectra estimates (measurements). The effective BT-product per record BT_{eff} is then given by

$$BT_{eff} = \frac{BT}{n_d} \tag{D.2}$$

where n_d is number of linear averages.

The Measurement Setup is shown in Fig. D.1.

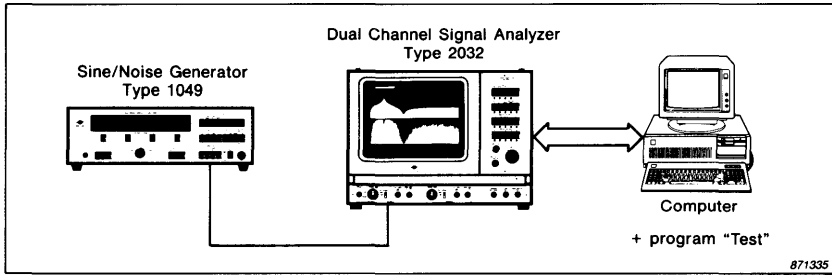

Fig. D.1. The instrumentation for experimental determination of the BT-product for FFT analysis

BT_{eff} per record	0% Overlap	50% Overlap	75% Overlap
Rectangular	0,954	0,674	0,368
Hanning	0,995	0,940	0,535
Kaiser-Bessel	1,009	0,996	0,628
Flat Top	0,990	1,000	0,994

Table D.1. Effective BT-product per record, when overlap analysis is performed (experimental values)

The number of averages (LIN), the overlap and the weighting function are chosen in the Measurement Setup of the 2032.

The readout of absolute (RMS) or relative (dB) values are chosen in the Display Setup.

The frequency interval (number of lines) and the number of estimates (measurements) are chosen in the programme.

Now the mean values and standard deviations from the autospectra at each frequency in the chosen frequency interval, as well as the mean value of these mean values and standard deviations are calculated in the computer.

A typical result is taken as the mean value of four experiments. In each experiment 100 estimates of autospectra, using 100 averages and 40 frequency lines, have been taken. Most of the results shown in Table D.I agree within 1 % of the theoretical values shown in Table 3 in Part I of this article.

Appendix E

Examples of User Defined Windows

The User Defined windows are implemented in the B & K Analyzers Types 2032/34 as

$$W(n) = \frac{2^E}{32768}\left[A_0 - A_1\cos\left(n\frac{2\pi}{N}\right) + A_2\cos\left(2n\frac{2\pi}{N}\right) - A_3\cos\left(3n\frac{2\pi}{N}\right) + A_4\left(4n\frac{2\pi}{N}\right)\right] \quad \text{(E.1)}$$

$0 \le n \le N - 1$

$N = 1024$ if in Zero Pad Mode
$N = 2048$ if not in Zero Pad mode

Notice the slightly different formulation from the rest of this article with a common scaling factor for all the window coefficients.

In the design of User Defined windows the following criterion must be used:

The exponent E must be an integer as small as possible, however large enough to fulfil Equation (E.2).

$$2^E \geqq \sum_{i=0}^{n} a_i \quad \text{(E.2)}$$

The coefficients Ai (E.I) are now calculated

$$A_i = 2^{(15 - E)} \cdot a_i \quad \text{(E.3)}$$

Hamming Window

The Hamming window is defined as

$w(t) = 1 - 0{,}84 \cos(2 \pi t)$ for $0 \le t < T$

$w(t) = 0$ elsewhere (E.4)

and has an Effective Noise Bandwidth of 1,3528 Δf.

The Hamming window can be implemented in the 2032 or 2034 using special parameters #6 to #12.

First the Noise Bandwidth is entered in special parameters #6 to #9 as

#6 and #8: 13528.
#7 and #9: -4.

Then the common exponent E in

#10: 1.

And finally the coefficients, here A_0 and A_1 in

#11: 2^{14} =16384 and
#12: $2^{14} \cdot 0{,}84$ = 13762.

This window is very similar to the Hanning Window, but has the special feature, that it suppresses the first sidelobe. However, the fall-off rate of the side-lobes is only 20 dB per decade compared to 60 dB per decade for the Hanning window. Fig. E.1 a) shows a "worst case" analysis of a sinusoid with Hamming weighting.

Blackman-Harris Window

The four term -92 dB Blackman-Harris window has the following coefficients:
$a_0 = 1$, $a_1 = 1{,}36...$, $a_2 = 0{,}39...$, $a_3 = 0{,}032....$ The Effective Noise Bandwidth is 2,00.. Δf.

The window is implemented in the 2032 or 2034 using the special parameters #6 to #14 as

#6 and #8: 2.
#7 and #9: 0.
#10: = 2.
#11: 2^{13} = 8192.
#12: $2^{13} \cdot 1{,}36$ = 11150.
#13: $2^{13} \cdot 0{,}39$ = 3226.
#10: $2^{13} \cdot 0{,}032$ = 267.

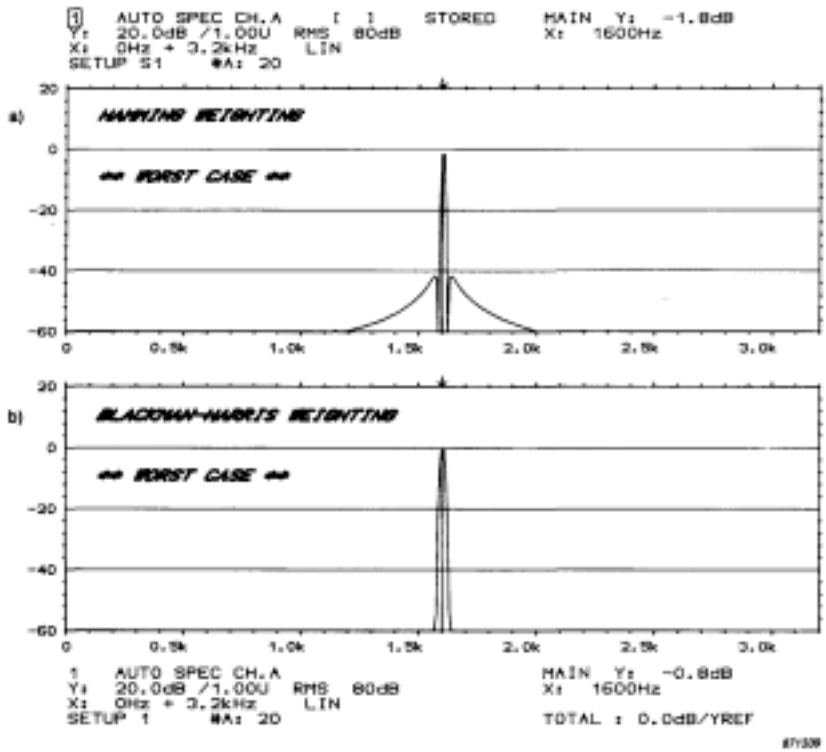

Fig. E.1. The "worst case", when analysing a sinusoid using a) Hamming window and b) Blackman-Harris window

The Blackman-Harris window has very much the same performance as the Kaiser-Bessel window Ref. [2] except that it suppresses the sidelobes more than 92 dB at a cost of an 11 % wider Noise Bandwidth. In Fig. E.1 b) a "worst case" analysis of a sinusoid with Blackman-Harris weighting is shown.

Appendix F

Picket Fence Effect

Whenever analysis with discrete fixed filters is performed, the spectrum is measured at the filter centre frequencies with a resolution given by the filter bandwidths. This is not only the case for DFT/FFT analysis, but in general when a bank of parallel filters or stepped filters are used for the analysis.

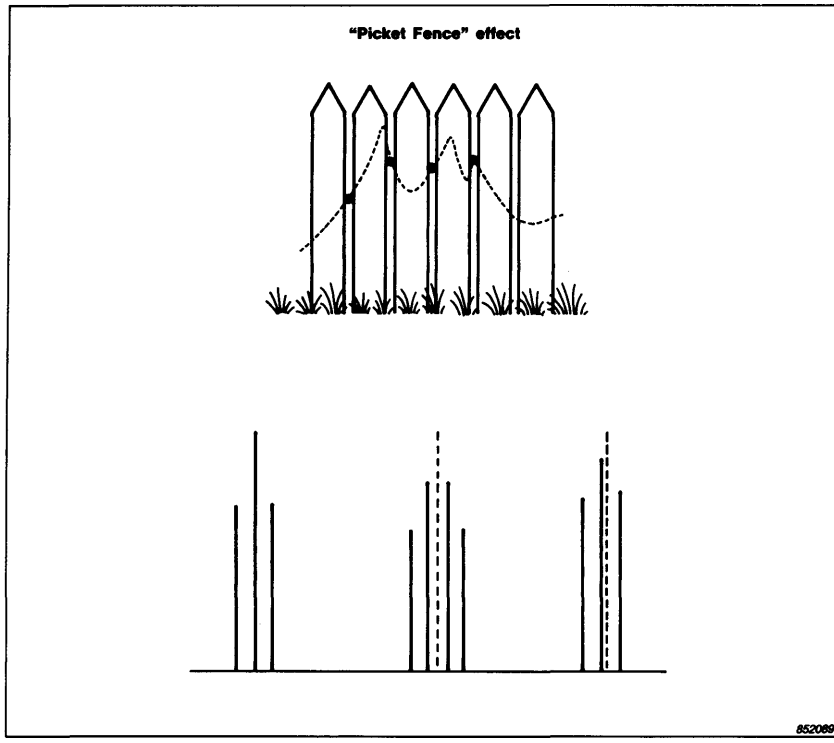

Fig. F.1. Illustration of Picket Fence Effect

The effect of only measuring the spectrum at discrete frequencies is referred to as the picket fence effect, since it is similar to viewing the continuous spectrum (measured with the given bandwidth) through a picket fence, see Fig. F.1.

As indicated in Figs. 7, 9, 12 and 16 (shown in Part I of this article) we will therefore in general get an error in both amplitude and frequency of the highest line in the spectrum of a frequency component. The amplitude error is limited by the ripple in the passband while the frequency error is limited by the line spacing Δf. The errors are referred to as picket fence effect errors. Only in the situation where the frequency component coincides with a centre frequency/line in the analysis both the amplitude and the frequency will be correct.

If we know or assume that it is a single and stable frequency component the errors can be compensated for by an interpolation technique on the well defined filter characteristics of the weighting functions, see Figs. 6, 8, 11 and 15 (in Part I of this article). The amplitude and frequency corrections can be calculated from the difference Δ, in dB, between the two highest lines around the peak. We will here limit the discussion to the Hanning window and Rectangular window, but similar formulae could be developed for other window functions.

The frequency correction, Δf_c Hz for Hanning Weighting is given by:

$$\Delta f_c = \frac{2 - 10\,\Delta^{\mathrm{dB}/20\mathrm{dB}}}{1 + 10^{\Delta\mathrm{dB}/20\mathrm{dB}}} \cdot \Delta f \qquad \text{(F.1)}$$

where Δf is the line spacing in the analysis.

The Equation F.1 is shown in graphical form in Fig. F.2 and is tabulated in Table F.1.

For Hanning Weighting, ΔdB has a maximum of 6 dB, when the frequency coincides exactly with an analysis line, and a minimum of zero dB, when it falls exactly between two lines.

The amplitude correction, ΔL dB for Hanning Weighting is given by

$$\Delta L = 20 \log \frac{\sin \pi\, \Delta f_c/\Delta f}{\pi\, \Delta f_c/\Delta f} \cdot \frac{1}{1-(\Delta f_c/\Delta f)^2} \qquad \text{(F.2)}$$

which is also shown in graphical forms in Fig. F.2 and is tabulated in Table F.1.

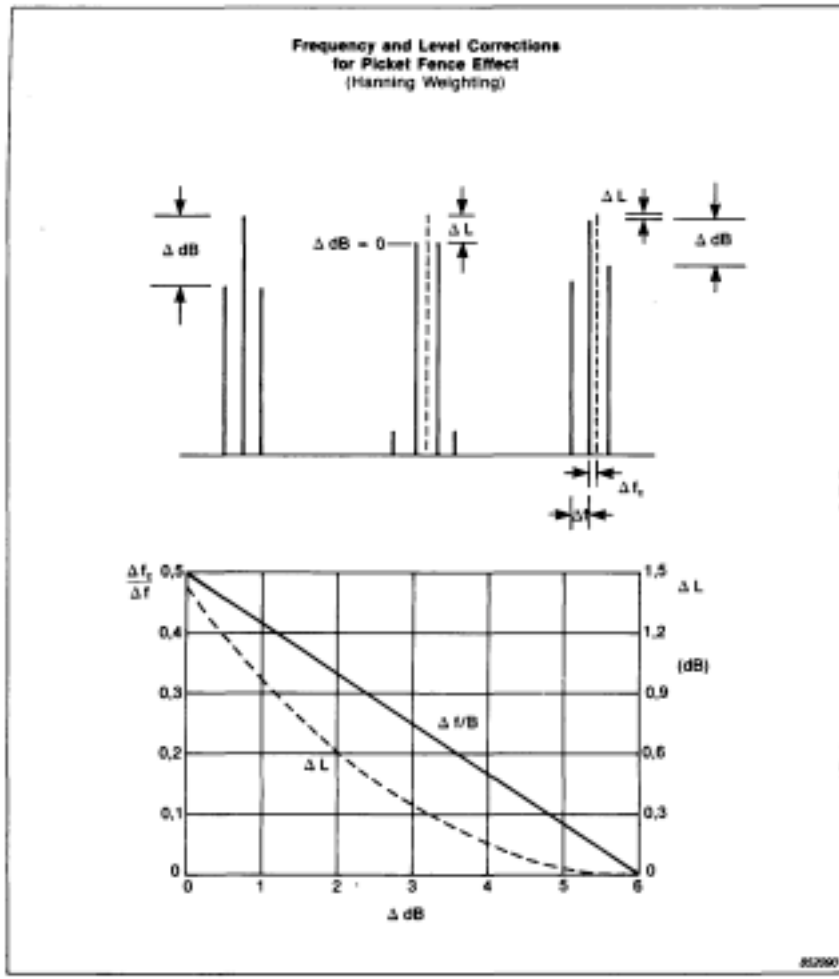

Fig. F.2. Amplitude and frequency compensation for picket fence effect with Hanning Weighting

For Hanning Weighting the amplitude correction, ΔL is 0 dB, when the frequency coincides exactly with an analysis line, which is indicated by a ΔdB equal to 6,0 dB. The amplitude correction is 1,42 dB, when ΔdB is equal to 0 dB, that is when the frequency of the signal is exactly between two lines.

ΔdB	ΔL	Δf_c
0.0	1.42	0.50
0.2	1.33	0.48
0.4	1.23	0.47
0.6	1.14	0.45
0.8	1.05	0.43
1.0	0.97	0.41
1.2	0.89	0.40
1.4	0.81	0.38
1.6	0.74	0.36
1.8	0.67	0.35
2.0	0.61	0.33
2.2	0.55	0.31
2.4	0.49	0.29
2.6	0.43	0.28
2.8	0.38	0.26

ΔdB	ΔL	Δf_c
3.0	0.33	0.24
3.2	0.29	0.23
3.4	0.25	0.21
3.6	0.21	0. 19
3.8	0. 18	0. 18
4.0	0. 14	0. 16
4.2	0. 12	0. 14
4.4	0.09	0. 13
4.6	0.07	0.11
4.8	0.05	0. 10
5.0	0.04	0.08
5.2	0.02	0.06
5.4	0.01	0.05
5.6	0.01	0.03
5.8	0.00	0.02
6.0	0.00	0.00

T01648GB0

Table F.1. Amplitude and frequency compensation for Picket Fence Effect with Hanning Weighting

Using this picket fence correction technique it is possible to achieve a frequency accuracy approximately 100 times finer than the line spacing. For cursor read out on 2032/34 the dB values used for these calculations can be found with two decimals rather than one in the Scratch Pad Memory octal addresses 1257 (the integer) and 1260 (the 10-exponent) for the upper graph, and 1357 (the integer) and 1360 (the 10-exponent) for the lower graph, see Fig. F.3.

For Rectangular Weighting the corresponding correction terms are for frequency

$$\Delta f_c = \frac{1}{1 + 10^{(\Delta dB / 20\ dB)}} \cdot \Delta f \qquad \text{(F.3)}$$

and for amplitude

$$\Delta L = 20 \log \frac{\left| \sin \pi \Delta f / \Delta f \right|}{\pi \Delta f_c / \Delta f} \qquad \text{(F.4)}$$

For system analysis where identification of resonance frequencies and dampings are essential similar techniques can be used. For lightly damped structures it is assumed that a resonance peak can be modelled by a single

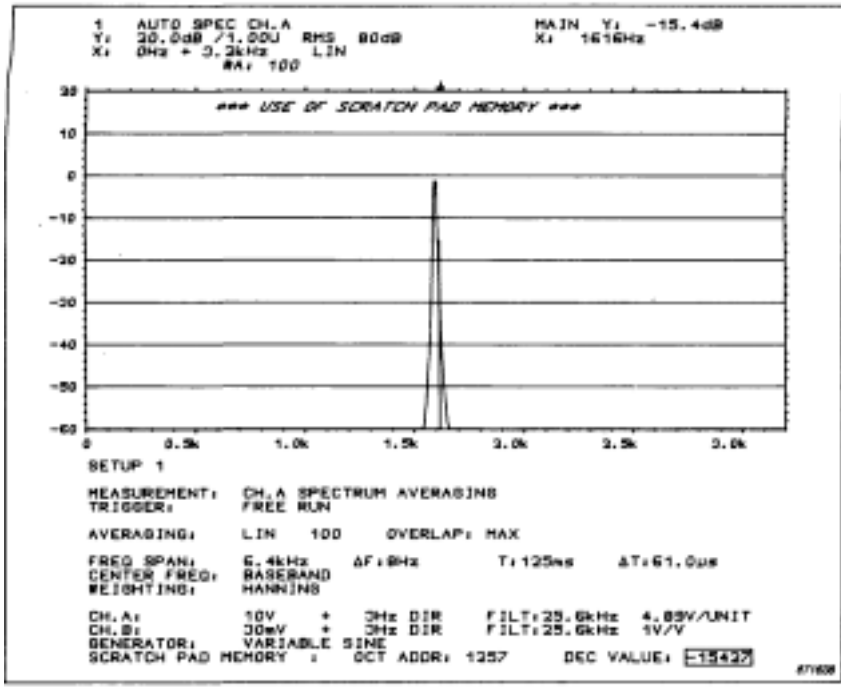

Fig. F.3. The use of scratch pad memory for readout of cursor values with higher accuracy

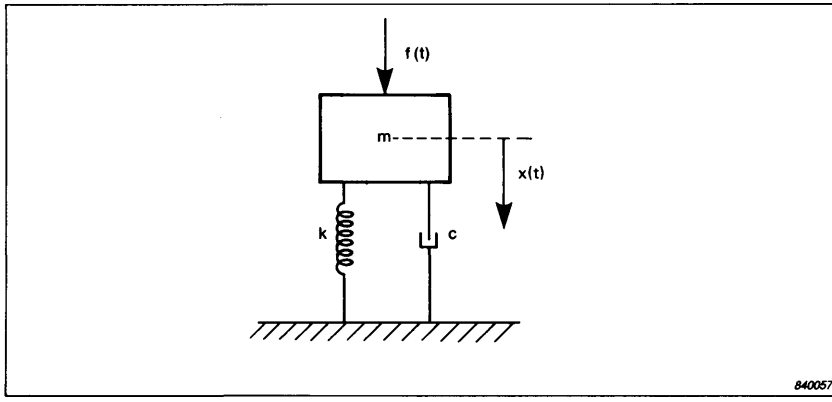

Fig. F.4. Mechanical Single Degree of Freedom (SDOF) model

degree of freedom (SDOF) model, see Fig. 4. Such a model, consisting of a mass, spring and a damper (Refs. [9 and 10]) has a Frequency Response Function as shown in Fig. F.5.

Using a curvefit technique where the mathematical SDOF model is fitted to the measured Frequency Response Function using the method of least squares error, the resonance frequency, the peak amplitude and the damping can be estimated with a degree of accuracy much better than the resolution of the FFT analysis allows. The assumption is that the measurement is free of leakage.

An example is shown in Fig. F.6 where the resolution, i.e. the line spacing is 4 Hz. Pseudo-random excitation is here used to avoid leakage in the analysis. The curvefit calculates the resonance frequency with a resolution at least 100 times higher than the FFT analysis. A zoom measurement verifies the results.

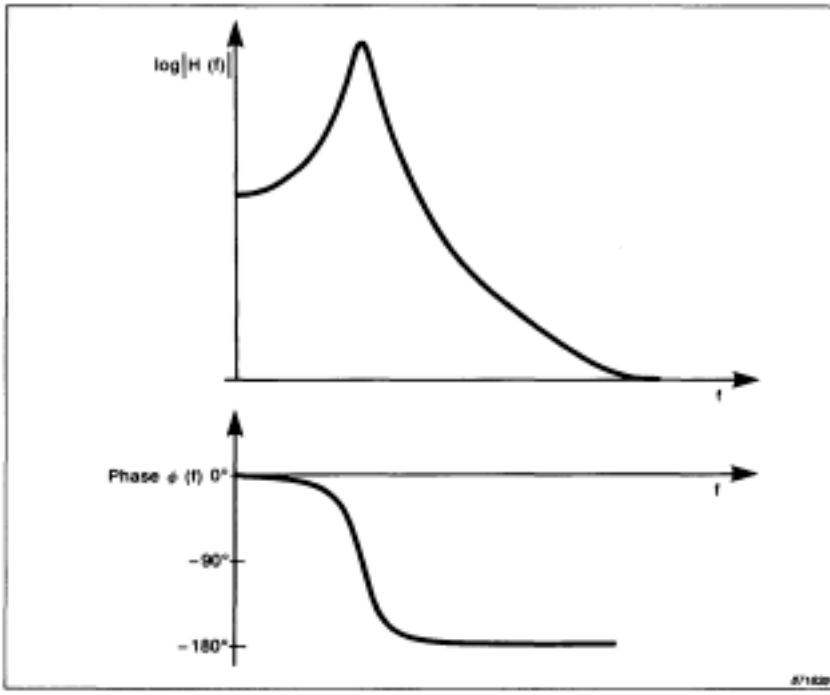

Fig. F.5. Logarithmic amplitude log $|H(f)|$ and phase $\phi(f)$ of the Frequency Response Function of a Single Degree of Freedom model

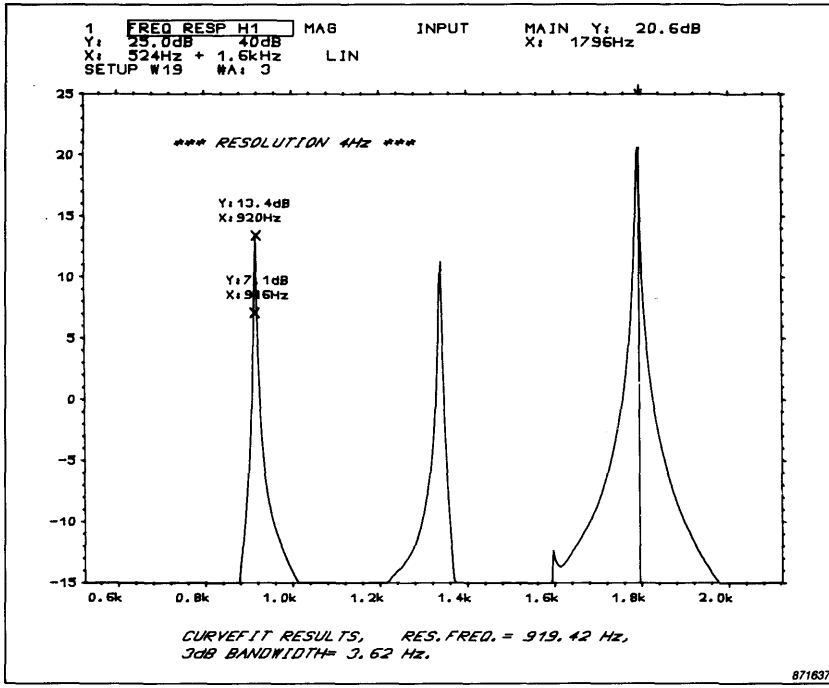

Fig. F.6. Estimation of resonance frequency and 3 dB bandwidth using a curvefit technique. Note that the line spacing in the analysis, Δf is 4 Hz

References

[1] Randall, R.B. *" Frequency Analysis* ", Brüel & Kjær, 1987

[2] Harris, F.J. *"On the Use of Windows for Harmonic Analysis with the Discrete Fourier Transform",* Proceedings of the IEEE, Vol. 66, No.1, January 1978, pp. 51-83.

[3] Welch, P.D. "*The use of Fast Fourier Transform for the estimation of power spectra: A method based on time averaging over short, modified periodigrams",* IEEE Trans. Audio Electro Acoust., Vol. AU-15, June 1967, pp.70-73

[4] Thrane, N. "*The Discrete Fourier Transform and FFT Analyzers",* B & K Technical Review, No.1-1979

[5] Thrane, N. "Zoom *FFT",* B & K Technical Review, No.2-1980

[6] Boyes, J.D. *"Effective Weighting of Overlapped Spectral Averaging",* B & K Internal Paper, 1980

[7] Brigham, E.G. "*The Fast Fourier Transform",* Prentice Hall Inc., New Jersey, 1974

[8] Papoulis, A. "*The Fourier Integral and its Applications",* McGraw-Hill Inc., New York, 1962

[9] Herlufsen, H. *"Dual Channel FFT Analysis, Part 1",* B & K Technical Review, No. 1-1984

[10] Herlufsen, H. *"Dual Channel FFT Analysis, Part* 2", B & K Technical Review, No.2-1984

Footnote *(from page 7)*

The linear averaging algorithm used in the analyzers is:

$$\overline{|Y(i)|^2} = \frac{1}{i}|Y(i)|^2 + \frac{i-1}{i}\overline{|Y(i-1)|^2}$$

for $1 \le i \le N$

Thus the averaging can be stopped with correctly scaled result after any number of averages without having to wait for the predefined number of averages, *N*, to be performed.

Acoustic Calibrator for Intensity Measurement Systems *

by Erling Frederiksen

Abstract

A description is given of an acoustic calibrator for intensity measurement systems which use microphones of the pressure principle. The calibrator produces signals corresponding to those detected by intensity probe microphones when the probe is placed in a free progressive sound wave with either 0° or 90° incidence.

In the 90°-mode the signals of the calibrator are equal with respect to magnitude and phase. This mode can be used for pressure-sensitivity calibration of intensity systems and for measurement of residual intensity index. Calibrators supplying this type of signals have previously been described in the literature.

However, for a more rigorous calibration it should be verified that the system responds correctly also to a phase difference between the sound field signals when this differs from zero. Therefore this calibrator has also the 0°-incidence mode. In this mode the calibrator signals are equal to the signals at two points in space within a free progressive sound wave. The phase difference corresponds to a certain distance between the points which means that it is proportional to frequency. The signal magnitudes and the phase difference have revealed high stability and calibration accuracy of 0,1 dB is possible. The calibrator can also be used for particle velocity calibration.

Sommaire

Tout d'abord la description d'une source sonore étalon pour les systèmes de mesure d'intensité acoustique par microphones sensibles à la pression

* First published in Internoise 1987

est donnée. Cette source produit des signaux correspondant à ceux qui sont détectés par les microphones des sondes, lorsque la sonde est exposée à une onde sonore progressive libre avec une incidence de 0 ou de 90°.

Dans le mode 90°, les signaux de la source sont identiques en amplitude et phase. Ce mode peut être utilise pour l'étalonnage de sensibilité en pression des systèmes d'intensité et pour les mesures d'index d'intensité résiduelle. Des sources délivrant ce type de signal ont déjà été décrites dans la littérature.

Cependant, pour un étalonnage plus rigoureux, il faut vérifier que le système répond correctement lorsqu'il y a une différence de phase entre les deux signaux. C'est pour cela que la source dispose d'un mode 0°, où les signaux provenant de la source sont identiques aux signaux engendrés en deux points de l'espace par une onde sonore progressive libre. La différence de phase correspond à une distance donnée entre les points, et elle est donc proportionnelle à la fréquence. L'amplitude des signaux et les différences de phase ont révélé qu'une très grande stabilité et qu'une précision de 0,1 dB sont possibles. La source peut aussi être utilisée pour les étalonnages de vitesse particulaire.

Zusammenfassung

Es wird ein akustischer Kalibrator für Intensitätsmeßsysteme mit Druckmikrofonen beschrieben. Das vom Kalibrator erzeugte Signal entspricht dem von einer Intensitätssonde aufgenommenen, wenn sich dieses in einem freien Schallfeld mit 0°- oder 90°- Einfall befindet.

Beim 90°-Betrieb erzeugt der Kalibrator Signale, die nach Betrag und Phase gleich sind. Hiermit läßt sich der Druckübertragungsfaktor des Intensitätsme#systems kalibrieren sowie der Remanenz-Intensitätsindex bestimmen. Kalibratoren, die diese Signalart erzeugen, wurden bereits früher in der Literatur beschrieben.

Für eine strengere Überprüfung der Kalibrierung sollte auch das Verhalten bei Signalen, die eine unterschiedliche Phasenlage besitzen, untersucht werden. Hierfür besitzt der Kalibrator den 0°-Betrieb. Hier erzeugt der Kalibrator Signale, die den Signalen an zwei räumlich verschiedenen Stellen einer sich frei fortpflanzenden Schallwelle entsprechen. Die Phasendifferenz entspricht einem gegebenen Abstand im Raum, d.h. sie ist frequenzproportional. Der Betrag und die Phasendifferenz der Signale sind hochstabil und eine Kalibriergenauigkeit von 0,1 dB ist möglich. Der Kalibrator läßt sich auch zur Teilchenschnelle-Kalibrierung einsetzen.

Introduction

Today measurement of sound intensity has proved its usefulness for noise analysis. Instruments are constantly improving, but as they are quite complex many users have desired means of calibration to gain further confidence in their measurement results.

Most systems use pressure microphones and practically all field calibrations made today are pressure calibrations of the system channels. In fewer cases the channels are also tested for equality of their phase responses - usually at one frequency only.

An acoustical calibrator for a far more extended calibration has been developed. According to known principles it can be used for pressure level calibration at 250 Hz and for phase check by measurement of residual intensity index between 10 Hz and 5 kHz.

In addition to these features the calibrator has an extra operation mode in which it produces signals for calibration of intensity and particle velocity sensitivity of instruments operated in these modes. This new mode is the main theme of this paper.

Operation Principle of Intensity System with Pressure Microphones

Most measurement systems which employ pressure microphones determine the instantaneous values of particle velocity, $u(t)$ and of the sound intensity, $I(t)$ in accordance with the following expressions:

$$u(t) = \int \frac{p_1(t) - p_2(t)}{\rho_o \Delta r_o} dt \; ; \quad I(t) = \frac{p_1(t) + p_2(t)}{2} \int \frac{p_1(t) - p_2(t)}{\rho_o \Delta r_o} dt$$

$P_1(t)$, $p_2(t)$: instantaneous values of the pressure signals
Δr_o, ρ_o: system parameters for microphone distance and air density

For sinusoidal signals the measured values of the particle velocity, u [rms] and of the time average value of sound intensity, $\bar{I}$ become:

$$u[\mathrm{rms}] = \frac{\left(\left[(P_1 + P_2)\sin\phi/2\right]^2 + \left[(P_1 - P_2)\cos\phi/2\right]^2\right)^{0,5}}{\omega \rho_o \Delta r_o}$$

$$\bar{I} = \frac{P_1 P_2 \sin\phi}{\omega \rho_o \Delta r_o}$$

P_1, P_2: rms-values of the sinusoidal pressure signals
ϕ, ω: phase angle between the pressure signals and angular frequency

Operation of the Sound Intensity Calibrator

The formulae above show that the measurement results are functions of four signal parameters. Therefore a calibrator has to produce signals for which these parameters are stable as functions of time and perform in a predictable way under common environmental conditions.

A calibrator which statisfies these requirements has been developed. It consists of a sound source and of a special coupler with two cavities, (a) and (b), see Fig. 1. The cavities have ports (1, 2 and 3) for connection of intensity probe microphones. One of the cavities (a) is directly connected to the source while the second cavity (b) is coupled to (a) via an acoustical coupling element which contains a resistance and a mass in series connection.

At low frequencies the acoustical network formed by the coupling element and by the compliance of cavity (b) creates cavity signals with a phase difference which is proportional to frequency and with magnitudes which are nearly equal. These properties exactly comply with the pressure at two points in a space where a plane sound wave is propagating. Thus for a pressure microphone probe the calibrator can simulate a free field wave with definable levels of sound pressure, particle velocity and intensity.

The coupler has been designed to create a phase difference corresponding to that valid for 50 mm microphone distance with an angle of zero degrees between the probe axis and the wave's propagation direction. The coupler properties are independent of the choice of sound source but a well defined source is needed for sensitivity calibration, therefore a piston-

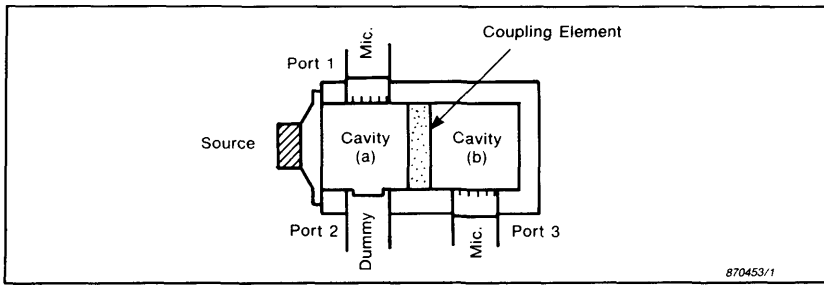

Fig.1. Principle of the intensity calibrator. The microphones are placed in the ports (1) and (3) for calibration of intensity sensitivity

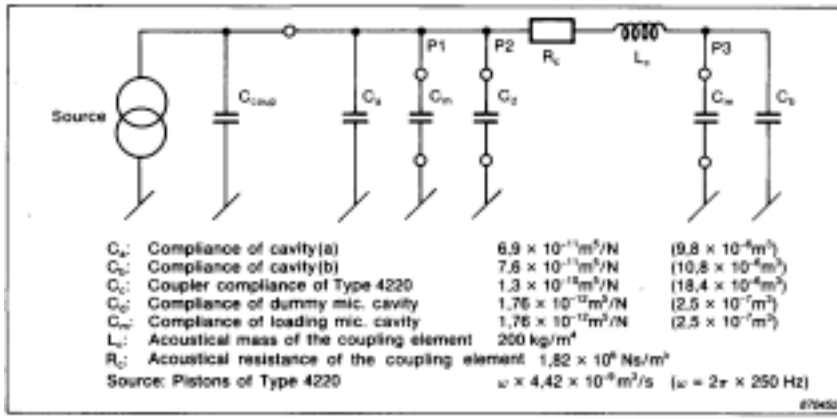

Fig.2. Model of the calibrator driven by the pistonphone with values valid at 1013 mbar and 20° C. The microphones are placed in the ports (1) and (3) for intensity or velocity calibration

phone, B & K Type 4220 was chosen for operations of this mode. See a model of the calibrator in Fig. 2.

The magnitude and phase differences between the pressure of the cavities, (b)-(a) have been measured and calculated, see Fig. 3 which also shows that within the range from a few Hz to about 500 Hz the phase difference between the ports is nearly equal to the free-field phase lag for points 50 mm apart. When driven by a pistonphone at 250 Hz the sound

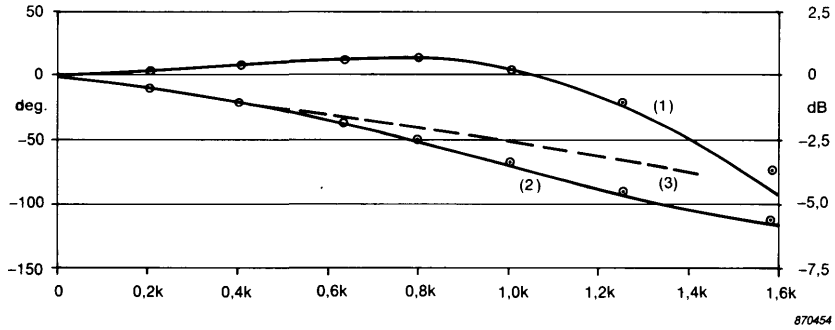

Fig. 3 Magnitude difference (1) and phase difference (2) between the pressure of the calibrator cavities, (b)-(a) were measured (curves) and calculated (points). The dotted line (3) shows the free-field phase lag for points 50 mm apart at 20° C

pressure levels of the cavities are nominally 118 dB therefore the particle velocity and intensity levels are also close to this value.

Due to the phase linearity with frequency the levels are not critical with respect to frequency. At 250 Hz the slopes are as small as + 0,7 x 10^{-3} dB/ Hz for intensity and + 1,5 x 10^{-3} dB/Hz for velocity.

Environmental Influences

The pressure and intensity levels as functions of the ambient pressure were measured with an FFT-analyzer and together with the particle velocity level they were also calculated by use of the model. The results are listed in the table below.

Attention should be paid to the agreement between the measured and the calculated results and to the fact that the intensity level is practically independent of the ambient pressure. Notice that the pressure level follows the ambient pressure (last line of the table) while the particle velocity level shows the same changes but in the opposite direction.

By measurement and calculation the temperature coefficient of the intensity level has been found to be + 0,024 dB/°C.

Amb. pressure, p_a	mbar	700	800	900	994	1000	1013
L_I measured	dB	-0,12	-0,07	-0,02	0	+0,01	-
L_I calculated	dB	-0,06	-0,03	-0,01	0	0	0
L_p cav.(a) measured	dB	-2,89	-1,80	-0,82	0	+0,05	-
L_p cav.(a) calculated	dB	-2,87	-1,79	-0,82	0	+0,05	+0,16
L_v calculated	dB	+2,93	+1,82	+0,83	0	-0,05	-0,15
20 log (P_a/994)	dB	-3,05	-1,89	-0,86	0	+0,05	+0,16

Notes for Application of the Calibrator

The calibrator is designed for laboratory as well as field use. The calibrator supplies sound pressure to the microphone diaphragms only. The calibrator works correctly with the newly introduced microphone types which are especially designed for intensity measurements and which have extremely low vent-sensitivity.

In the calibration mode for intensity sensitivity only very small errors will occur with ordinary measurement microphones while significant errors might occur in the mode for measurement of residual intensity index, especially at low frequencies.

Accuracy and Calibration of the Intensity Calibrator

Determination of the calibrator's intensity and particle velocity levels requires calibration of sound pressure, frequency and of the phase difference between the cavities which is more simple to measure than might be expected as microphones with known phase characteristics are not needed.

Calibration can be made with any two microphones which load the coupler correctly, i.e. with 250 mm^3. During the first phase measurement the microphones are inserted arbitrarily in the ports (1) and (3) while they are interchanged before the second measurement. The difference between the results is twice the phase difference between the cavities. The method eliminates a possible phase difference between the channels of the applied phase meter. The resulting calibration levels are found by inserting the measured values in the formulae given under the discussion of the measurement principle.

An accuracy of the intensity calibration level better than 0,15 dB is rather easy to obtain and seems relevant in practice as artificial stability tests have given very promising results for the calibrator.

Conclusion

An intensity calibrator with a possible accuracy of 0,1 dB has been developed. The calibrator can simulate two angles of sound incidence on the intensity probe, 0° or 90°. In the 0°-mode sensitivity of measurement systems can be calibrated while in the 90°-mode the residual intensity index can be measured.

It might be necessary to correct the calibrator's intensity level for the temperature but the ambient pressure has practically no influence at all.

The principle is new but the properties of the calibrator have been measured under different environmental conditions and a model has been worked out. The good agreement between the behaviour of the calibrator and the model shows that all significant physical effects are known.

For assistance with the experiments the author wishes to thank A. Halfdaner.

References

[1] Rasmussen, G., Brock, M. "*Transducers for intensity measurements",* ICA, Paris 83

[2] Frederiksen E. *"Pressure microphones for intensity measurements with significantly improved phase properties",* ICA, Toronto, '86

Previously issued numbers of Brüel & Kjær Technical Review

(Continued from cover page 2)

4-1982 Sound Intensity (Part II Instrumentation and Applications)
Flutter Compensation of Tape Recorded Signals for Narrow Band Analysis
3-1982 Sound Intensity (Part I Theory).
2-1982 Thermal Comfort.
1-1982 Human Body Vibration Exposure and its Measurement.
4-1981 Low Frequency Calibration of Acoustical Measurement Systems.
Calibration and Standards. Vibration and Shock Measurements.
3-1981 Cepstrum Analysis.
2-1981 Acoustic Emission Source Location in Theory and in Practice.
1-1981 The Fundamentals of Industrial Balancing Machines and Their Applications.
4-1980 Selection and Use of Microphones for Engine and Aircraft Noise Measurements.
3-1980 Power Based Measurements of Sound Insulation.
Acoustical Measurement of Auditory Tube Opening.
2-1980 Zoom-FFT.
1-1980 Luminance Contrast Measurement.
4-1979 Prepolarized Condenser Microphones for Measurement Purposes.
Impulse Analysis using a Real-Time Digital Filter Analyzer.
3-1979 The Rationale of Dynamic Balancing by Vibration Measurements.
Interfacing Level Recorder Type 2306 to a Digital Computer.
2-1979 Acoustic Emission.

Special technical literature

Brüel & Kjær publishes a variety of technical literature which can be obtained from your local Brüel & Kjær representative.
The following literature is presently available:

○ Mechanical Vibration and Shock Measurements (English), 2nd edition
○ Modal Analysis of Large Structures-Multiple Exciter Systems (English)
○ Acoustic Noise Measurements (English), 3rd edition
○ Architectural Acoustics (English)
○ Noise Control (English, French)
○ Frequency Analysis (English)
○ Electroacoustic Measurements (English, German, French, Spanish)
○ Catalogues (several languages)
○ Product Data Sheets (English, German, French, Russian)

Furthermore, back copies of the Technical Review can be supplied as shown in the list above. Older issues may be obtained provided they are still in stock.

Brüel & Kjær

DK-2850 Nærum · Denmark · Telephone: +45 2800 500 · Telex: 37316 bruka dk · Fax.: 02 80 14 05

ISSN 007–2621

BV 0032–11

Printed in Denmark by Nærum Offset